3270–3276 *Nucleic Acids Research, 2001, Vol. 29, No. 15*

The weak interdomain coupling observed in the 70 kDa subunit of human replication protein A is unaffected by ssDNA binding

Gary W. Daughdrill*, Jennifer Ackerman[1], Nancy G. Isern[2], Maria V. Botuyan[3], Cheryl Arrowsmith[3], Marc S. Wold[4] and David F. Lowry[2]

Department of Microbiology, Molecular Biology and Biochemistry, University of Idaho, PO Box 443052, Life Science South Room 142, Moscow, ID 83844-3052, USA, [1]PO Box 16204, Stanford University, Stanford, CA 94309, USA, [2]Environmental Molecular Sciences Laboratory, Pacific Northwest National Laboratory, 902 Battelle Boulevard, Richland, WA 99352, USA, [3]Division of Molecular and Structural Biology, Ontario Cancer Institute and Department of Medical Biophysics, University of Toronto, 610 University Avenue, Toronto, ON M5G 2M9, Canada and [4]Department of Biochemistry, University of Iowa College of Medicine, 51 Newton Road, Iowa City, IA 52240-1109, USA

Received March 15, 2001; Revised and Accepted June 8, 2001

ABSTRACT

Replication protein A (RPA) is a heterotrimeric, multifunctional protein that binds single-stranded DNA (ssDNA) and is essential for eukaryotic DNA metabolism. Using heteronuclear NMR methods we have investigated the domain interactions and ssDNA binding of a fragment from the 70 kDa subunit of human RPA (hRPA70). This fragment contains an N-terminal domain (NTD), which is important for hRPA70–protein interactions, connected to a ssDNA-binding domain (SSB1) by a flexible linker ($hRPA70_{1–326}$). Correlation analysis of the amide ^{1}H and ^{15}N chemical shifts was used to compare the structure of the NTD and SSB1 in $hRPA70_{1–326}$ with two smaller fragments that corresponded to the individual domains. High correlation coefficients verified that the NTD and SSB1 maintained their structures in $hRPA70_{1–326}$, indicating weak interdomain coupling. Weak interdomain coupling was also suggested by a comparison of the transverse relaxation rates for $hRPA70_{1–326}$ and one of the smaller hRPA70 fragments containing the NTD and the flexible linker ($hRPA70_{1–168}$). We also examined the structure of $hRPA70_{1–326}$ after addition of three different ssDNA substrates. Each of these substrates induced specific amide ^{1}H and/or ^{15}N chemical shift changes in both the NTD and SSB1. The NTD and SSB1 have similar topologies, leading to the possibility that ssDNA binding induced the chemical shift changes observed for the NTD. To test this hypothesis we monitored the amide ^{1}H and ^{15}N chemical shift changes of $hRPA70_{1–168}$ after addition of ssDNA. The same amide ^{1}H and ^{15}N chemical shift changes were observed for the NTD in $hRPA70_{1–168}$ and $hRPA70_{1–326}$. The NTD residues with the largest amide ^{1}H and/or ^{15}N chemical shift changes were localized to a basic cleft that is important for hRPA70–protein interactions. Based on this relationship, and other available data, we propose a model where binding between the NTD and ssDNA interferes with hRPA70–protein interactions.

INTRODUCTION

DNA metabolism is the coordinated replication, recombination and repair that occurs during the cell cycle, ensuring transmission of a robust and error-free copy of the genome. Replication protein A (RPA) is a heterotrimeric protein that is essential for multiple processes during eukaryotic DNA metabolism (1). The three subunits of RPA are 70, 30 and 14 kDa in size and homologs for these subunits have been identified in all eukaryotes for which sequence data are available (1–4). One essential RPA function during DNA metabolism is single-stranded (ss)DNA binding. To perform this function the human homolog of the 70 kDa subunit of RPA (hRPA70) contains two high affinity ssDNA-binding domains between residues 181 and 422 (SSB1 and SSB2 in Fig. 1; 1,5,6). hRPA70 also contains a DNA-binding domain that is important for damage recognition. This domain is C-terminal of residue 422 and requires a metal, possibly Zn^{2+}, to function (ZBD in Fig. 1; 1,5,6). In addition, the N-terminal 108 amino acids of hRPA70 form a discrete structural domain that is responsible for many of the specific hRPA70–protein interactions that occur during DNA metabolism (NTD in Fig. 1; 5,7–11). The NTD stimulates the activity of DNA polymerase α and binds to the transcriptional activators GAL4, VP16 and p53 (5,7–10). Finally, residues 109–181 of hRPA70 form a flexible linker connecting the NTD to SSB1 (11).

To further the current understanding of how hRPA70 functions during DNA metabolism heteronuclear magnetic resonance (NMR) methods were used to investigate the domain interactions and ssDNA binding of an hRPA70 fragment containing the NTD, the flexible linker and SSB1

*To whom correspondence should be addressed. Tel: +1 208 885 9230; Fax: +1 208 885 6518; Email: gdaugh@uidaho.edu

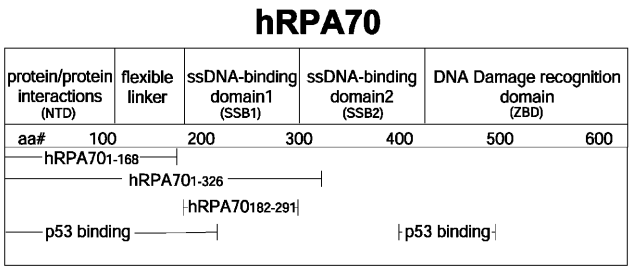

Figure 1. Schematic diagram of the 70 kDa subunit of human RPA showing the relative positions of the functional domains in the linear sequence. Also shown are the positions of the three fragments used in this study, $hRPA70_{1–168}$, $hRPA70_{1–326}$ and $hRPA70_{181–291}$, and the regions of hRPA70 required for p53 binding.

($hRPA70_{1–326}$). The structural model of $hRPA70_{1–326}$ for this work was the NMR-derived model of $hRPA70_{1–168}$ and the X-ray-derived model of the $hRPA70_{181–422}$–ssDNA complex (11,12). Both the NTD and SSB1 globular domains are structurally homologous oligonucleotide-binding folds with no sequence homology.

The ability of ssDNA binding by SSB1 to induce structural changes in the NTD was investigated under the hypothesis that interdomain coupling, i.e. a direct interaction between the surfaces of the two domains, modulates hRPA70–protein and/or hRPA70–ssDNA interactions. This hypothesis could explain the observation that ssDNA binding by hRPA70 interferes with NTD–protein interactions (13). Alternative hypotheses are that ssDNA modulates NTD interactions with an hRPA70 domain other than SSB1 or with one of the other two hRPA subunits or that the NTD interacts directly with ssDNA. However, previous binding studies failed to detect an interaction between the NTD and ssDNA, rendering the latter hypothesis unlikely. Interestingly, our study shows that the NTD can interact weakly with ssDNA and that NTD residues with the largest chemical shift changes after addition of ssDNA cluster near a basic cleft that is also important for NTD–protein interactions.

MATERIALS AND METHODS

Protein expression and purification

The $hRPA70_{1–326}$, $hRPA70_{1–168}$ and $hRPA70_{182–291}$ fragments were expressed in *Escherichia coli* and purified as described (11,14). The following changes were made to the published protocols. Standard minimal medium was used for bacterial growth, which included ^{15}N-labeled ammonium chloride and ^{13}C-labeled glucose when necessary. A buffer containing 20 mM Tris–HCl, pH 7.4, 50 mM KCl, 0.02% sodium azide and 5 mM DTT was used for cell lysis and chromatography. This was also the final buffer used for NMR experiments on the three fragments. The homogeneity of the NMR spectra as well as gel analysis was used to verify the purity and stability of samples.

Oligonucleotide synthesis

Four ssDNA oligomers were synthesized using an Applied Biosystems DNA synthesizer model 392. Three of these oligomers contained all thymines with lengths of 8, 10 and 12 bases (dT_8, dT_{10} and dT_{12}). The fourth oligomer was a nonanomer with sequence CCAATAACC (9mer). After synthesis all oligomers were lyophilized overnight to remove ammonia, then each oligomer was incubated in 600 µl of 300 mM KCl for 1 h at 55°C. The oligomers were then purified by passage over a G25 desalting column using deionized nanopure water as the eluent. The samples were then lyophilized and resuspended in 50 µl of the same buffer used for protein purification. Final concentrations of the purified samples ranged from 8 to 20 mM.

NMR experiments

All NMR experiments were performed on Varian spectrometers at 600–800 mHz. Two-dimensional, gradient-enhanced ^{1}H-^{15}N HSQC spectra were acquired on uniformly ^{15}N- or $^{13}C/^{15}N$-labeled $hRPA70_{1–168}$, $hRPA70_{1–326}$ and $hRPA70_{182–291}$ samples in 90% H_2O/10% D_2O (15,16). The backbone nuclear resonances ($^{1}H^{N}$, ^{15}N, $^{13}C^{\alpha}$, $^{13}C'$) and $^{13}C^{\beta}$ nuclear resonances were tentatively assigned for $hRPA70_{1–168}$ and $hRPA70_{182–291}$, in the absence of ssDNA, using data from a combination of the 3D HNCACB (17,18), 3D CBCA(CO)NH (17–19) and/or 3D HNCO (17–20) experiments. The backbone nuclear resonances ($^{1}H^{N}$, ^{15}N) of $hRPA70_{1–326}$ were assigned, in the absence of ssDNA, by comparison with the assigned ^{1}H-^{15}N HSQC spectra of $hRPA70_{1–168}$ and $hRPA70_{182–291}$. This approach assumed a minimal perturbation in the ^{1}H-^{15}N HSQC spectra of $hRPA70_{1–326}$ compared with spectra of the individual globular domains. Resonance assignments for $hRPA70_{1–326}$ were primarily confined to M1–A128 of the NTD and S182–D291 of SSB1. Spectral overlap and intermediate exchange prevented unambiguous resonance assignments for most of the linker residues, with the exception of V106–Y118, G121, G123 and A128. In addition, 15 resonances were assigned between D292 and Y326. These 15 resonances correspond to residues in a region that connects SSB1 to SSB2 and are unfolded based on the lack of ^{1}H and C^{α} chemical shift dispersion.

The backbone nuclear resonances ($^{1}H^{N}$, ^{15}N, $^{13}C^{\alpha}$) and $^{13}C^{\beta}$ nuclear resonances of $hRPA70_{1–326}$ bound to dT_8 were initially tentatively assigned by assuming a minimal change in chemical shifts upon addition of ssDNA and partly confirmed using 3D HNCACB. The backbone nuclear resonances ($^{1}H^{N}$, ^{15}N, $^{13}C^{\alpha}$) and $^{13}C^{\beta}$ nuclear resonances of $hRPA70_{1–326}$ bound to the 9mer were also assigned by assuming a minimal change in spectrum and using 3D CBCA(CO)NH to determine whether the possible amino acid types that are N-terminal are consistent with the amino acid type of the resonance that shifts. The assumption of minimal change in spectrum has been used several times to assign perturbed spectra and the strategy generates the most conservative conclusions about the nature of the perturbation (21–25). Using the minimal change criterion, 3D HNCACB and CBCA(CO)NH, it was possible to make ^{1}H and ^{15}N resonance assignments for 169 of the 217 possible resonances from the NTD and SSB1. The backbone nuclear resonances ($^{1}H^{N}$, ^{15}N) of $hRPA70_{1–326}$ bound to dT_{10} and dT_{12} were assigned by comparison with the ^{1}H-^{15}N HSQC spectrum of $hRPA70_{1–326}$ bound to dT_8. This assignment approach assumes a consistent direction, but not magnitude, in the ^{1}H and ^{15}N chemical shifts when the length of the thymine oligomers was increased. Transverse relaxation experiments were a variation of those developed by Kay *et al.* (26). A series

Table 1. Statistics for chemical shift correlation plots

Correlation	Horizontal axis	Vertical axis	Slope (*M*)	Correlation coefficient (*r*)
A	$hRPA70_{1–326}$ (^1H p.p.m.)	$hRPA70_{182–291}$ (^1H p.p.m.)	0.99	1.00
B	$hRPA70_{1–326}$ (^{15}N p.p.m.)	$hRPA70_{182–291}$ (^{15}N p.p.m.)	1.00	1.00
C	$hRPA70_{1–326}$ (^1H p.p.m.)	$hRPA70_{1–168}$ (^1H p.p.m.)	1.00	1.00
D	$hRPA70_{1–326}$ (^{15}N p.p.m.)	$hRPA70_{1–168}$ (^{15}N p.p.m.)	1.00	1.00
E	$hRPA70_{1–168}$ + dt_{10} (δ^1H p.p.m.)	$hRPA70_{1–326}$ + dt_8 (δ^1H p.p.m.)	0.78	0.87

of ^1H-^{15}N HSQC spectra were collected for $hRPA70_{1–168}$ and $hRPA70_{1–326}$ with relaxation delays varying from 5 to 50 ms in 5 ms increments. Relaxation rates were determined by fitting the decaying intensities from these experiments to a single decaying exponential function. All NMR data were processed using the FELIX97 program distributed by MSI (San Diego, CA).

ssDNA titration experiments

In this study titration experiments with $hRPA70_{1–326}$ were performed with the four ssDNA oligomers mentioned above. The dT_{10} oligomer was also used for a titration experiment with $hRPA70_{1–168}$. The concentrations of the $hRPA70_{1–326}$ and $hRPA70_{1–168}$ samples were between 0.5 and 1.0 mM. Four equal amounts of ssDNA were added to each protein sample until the concentration of ssDNA was 2 mM. ^1H-^{15}N HSQC spectra were acquired and analyzed after each addition of ssDNA. The pH of the NMR sample before and after one of the titrations was directly measured and did not change.

RESULTS AND DISCUSSION

Conservation of the NTD and SSB1 structures in $hRPA70_{1–326}$

To test if the NTD and/or SSB1 structures adopted a new conformation in the $hRPA70_{1–326}$ fragment, the amide ^1H and ^{15}N chemical shifts from the ^1H-^{15}N HSQC spectra of $hRPA70_{1–168}$, $hRPA70_{182–291}$ and $hRPA70_{1–326}$ were correlated. Figure 1 shows the positions of these fragments in the linear sequence of hRPA70. The correlation coefficients and slopes for the NTD and SSB1 resonances in the context of the three fragments are listed in Table 1. The values are close or equal to one, implying that there are minimal changes in the structures of the two domains when they are connected by the flexible linker. The largest amide ^1H and/or ^{15}N chemical shift changes occurred for NTD residues M57 ($^1H\delta\Delta$ = 0.05 p.p.m.) and L87 ($^{15}N\delta\Delta$ = 0.42 p.p.m.) and for SSB1 residues W197 ($^1H\delta\Delta$ = 0.06 p.p.m.) and F269 ($^{15}N\delta\Delta$ = 0.65 p.p.m.). From this analysis we conclude that any coupling that exists between the NTD and SSB1 in $hRPA70_{1–326}$ is weak. Of course, we cannot rule out the possibility of coupling between the NTD and SSB2, the ZBD or the other two subunits of hRPA.

The two globular domains of $hRPA70_{1–326}$ rotate independently

Transverse relaxation experiments were performed on $hRPA70_{1–168}$ and $hRPA70_{1–326}$, with the expectation that the lack of a strong direct interaction between the two domains would give rise to similar transverse relaxation rates for $hRPA70_{1–326}$ compared with $hRPA70_{1–168}$ (27). ^{15}N transverse relaxation rates (R_2) were calculated by fitting the residue-specific intensities from a series of relaxation experiments to a single decaying exponential function. Figure 2 shows a plot of R_2 for the NTD in $hRPA70_{1–168}$ and $hRPA70_{1–326}$ versus residue number. Unambiguous rate determinations were possible for 94 of the N-terminal 114 residues of $hRPA70_{1–168}$ and for 78 of the N-terminal 117 residues of $hRPA70_{1–326}$.

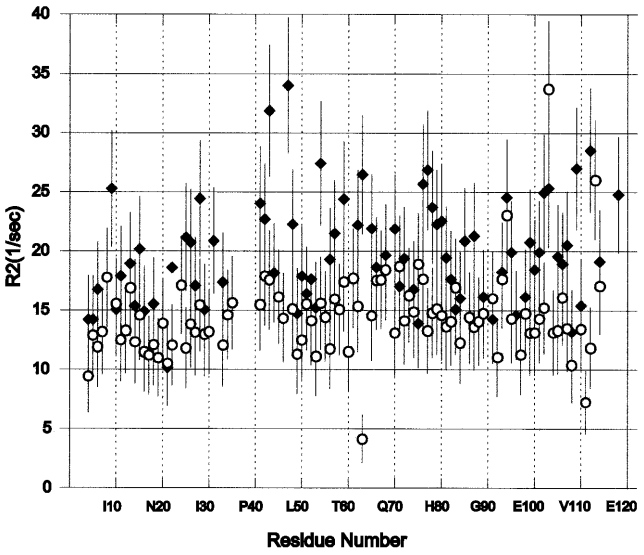

Figure 2. Plot showing the residue-specific transverse relaxation rates for 94 of the N-terminal 114 $hRPA70_{1–168}$ residues (circles) and for 78 of the N-terminal 117 $hRPA70_{1–326}$ residues (diamonds).

The mean value for the 94 rates from $hRPA70_{1–168}$ was 14.5 ± 3.5 s^{-1} and for the 78 rates from $hRPA70_{1–326}$ was 19.7 ± 4.5 s^{-1}. This increase seems unusually small considering that the molecular weight of $hRPA70_{1–326}$ is almost double the molecular weight of $hRPA70_{1–168}$. The small increase in the mean R_2 suggests that the linker is still flexible in $hRPA70_{1–326}$ and rotational diffusion of the two domains is relatively independent. A much larger increase in R_2 was expected if the NTD and SSB1 were tightly bound. The observed increase is further evidence of weak coupling between the two domains.

The global change in transverse relaxation rates for the NTD, with and without SSB1, is quite small. However, a number of residue-specific changes were greater than the average. For instance, residues R43, S54, N63, C77 and I112 show increases in their transverse relaxation rates that are >10 s^{-1}.

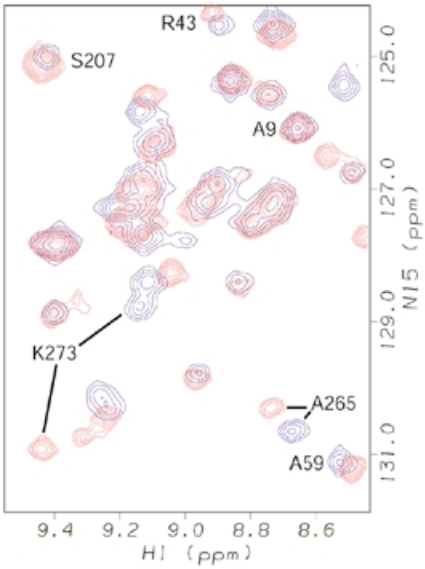

Figure 3. Overlay of a selected region from the ^{1}H-^{15}N HSQC spectra of $hRPA70_{1–326}$ (blue resonances) and $hRPA70_{1–326}$ bound to dT_{12} (red resonances). Representative resonances for residues in the two domains of $hRPA70_{1–326}$ are labeled. ^{1}H chemical shifts on the p.p.m. scale are on the horizontal axis and ^{15}N chemical shifts on the p.p.m. scale are on the vertical axis.

Localized changes in the transverse relaxation rates indicate that these residues explore a larger range of conformations and/or the exchange rate between conformations is decreased (28,29). It is unclear how the addition of SSB1 to the flexible linker results in such a large increase in R_2 for specific residues in the NTD.

NMR analysis of $hRPA70_{1–326}$ binding to ssDNA

The amide ^{1}H and ^{15}N chemical shifts of $hRPA70_{1–326}$ were monitored before and after addition of the ssDNA oligomers described in Materials and Methods. Figure 3 shows an overlay of the resonances from a selected region of the ^{1}H-^{15}N HSQC spectra of $hRPA70_{1–326}$ before and after addition of dT_{12} to 2 mM, shown respectively in blue and red. Figure 3 shows that chemical shift changes were observed for specific residues in both the NTD and SSB1. For instance, chemical shift changes were observed for the resonances of A59 and R43 from the NTD as well as K273 and A265 from SSB1. A difference in the size of the chemical shift changes for the NTD resonances, compared with SSB1 resonances, is consistently observed throughout the spectra.

The amide ^{1}H and ^{15}N chemical shift changes that occurred upon binding of $hRPA70_{1–326}$ to dT_8, the 9mer and dT_{12} were measured and are plotted in Figure 4. Figure 4A and C show the amide ^{1}H and ^{15}N chemical shift changes for the assigned resonances from the NTD of $hRPA70_{1–326}$, respectively. Figure 4B and D show the amide ^{1}H and ^{15}N chemical shift changes for the assigned resonances from SSB1 of $hRPA70_{1–326}$, respectively. In all four panels the chemical shift differences, in p.p.m., are plotted on the vertical axis and the residue numbers are plotted on the horizontal axis. The chemical shift differences were taken as the chemical shift of a given resonance in the presence of 2 mM ssDNA minus the chemical shift of a given resonance in the absence of ssDNA. In all of the panels in Figure 4 red circles correspond to the chemical shift changes that occurred upon binding to dT_8, blue squares correspond to the chemical shift changes that occurred upon binding to the 9mer and green crosses correspond to the chemical shift changes that occurred upon binding to dT_{12}.

The largest amide ^{1}H and ^{15}N chemical shift changes observed for SSB1 were for residues F269–T279. Other SSB1 residues with large ^{15}N chemical shift changes include I209–T211, R216–E218, K220 and F222. In the crystal structure of $hRPA70_{181–422}$ bound to dC_8, residues F269–T279 are located in β-strands 4 and 5, which are part of the ssDNA-binding pocket (12). However, the only residues from F269–T279 directly contacting the DNA are F269 and E277. The large amide chemical shift changes observed for all the residues from F269 to T279 are consistent with a change in the structure of β-strands 4 and 5 (Fig. 5).

The largest amide ^{1}H chemical shift changes observed for the NTD were for residues T35, Y42, A59–L62 and D89 and the largest amide ^{15}N chemical shift changes were for residues T34, R41, T86, R91, V93 and Y118. In the solution structure of $hRPA70_{1–168}$ residues A59–L62 are located in a turn between β-strand 3 and α-helix 2, which is at the base of the positively charged cleft (11). T34, T35, R41 and T86 are located in β-strands 1, 2 and 4, respectively, which form the ridges of the basic cleft. It appears that all NTD residues with significant amide ^{1}H and ^{15}N chemical shift changes are localized in the basic cleft (Fig. 5).

It is interesting that different lengths of ssDNA do not affect the magnitude of the change in proton chemical shift for the SSB1 resonances, while longer ssDNAs caused larger shifts in NTD resonances (Fig. 4). This observation indicates that NTD binding to ssDNA is unsaturated and in fast exchange, while at the same ssDNA concentration SSB1 binding is saturated and in slow exchange. Such exchange regimes for the two domains are consistent with the published affinities of the fragments for ssDNA (30): $RPA70_{1–326}$ has a sub-micromolar dissociation constant while $RPA70_{1–168}$ binding is so weak it could not be detected. These results, together with the assumption of a diffusion-controlled on rate, imply that under the present conditions ssDNA binding by the NTD would be unsaturated and in fast exchange while binding by SSB1 would be saturated and in slow exchange. How is it that one domain of a molecule can have such different spectral sensitivity to ssDNA than another domain of the same molecule? A possible explanation is that because the SSB1 domain only binds three nucleotides, the NTD domain, like SSB2 in the co-crystal (12), could bind the same oligomer as the SSB1 domain. While SSB1 tightly binds a particular ssDNA molecule, the NTD is binding and releasing the same ssDNA molecule with a rate that is fast on the NMR chemical shift timescale. Longer ssDNA oligomers contain more NTD binding sites so the effective concentration of ssDNA is higher, causing increasing chemical shift changes for NTD but not SSB1.

NMR and correlation analysis of $hRPA70_{1–168}$ binding to ssDNA

The amide ^{1}H and ^{15}N chemical shift changes observed for the NTD resonances in $hRPA70_{1–326}$ resulted from either a direct interaction with ssDNA or an interaction with SSB1 that was

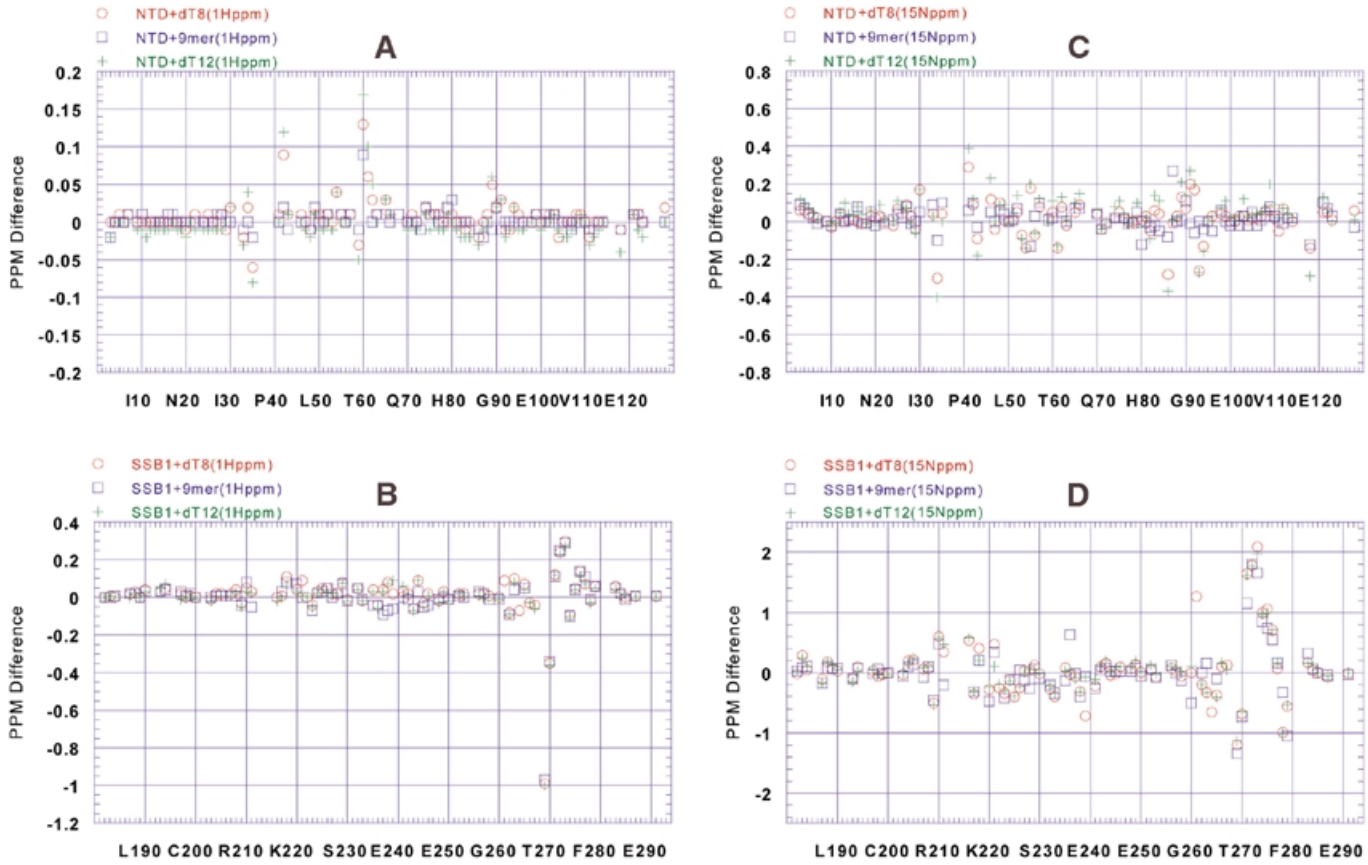

Figure 4. (**A**) Plot showing the amide ^{1}H chemical shift changes in p.p.m. for the assigned resonances from the NTD of hRPA70$_{1–326}$ when bound to dT$_{8}$ (red circles), the 9mer (blue squares) and dT$_{12}$ (green crosses) on the vertical axis versus residue number on the horizontal axis. (**B**) Plot showing the amide ^{1}H chemical shift changes in p.p.m. for the assigned resonances from SSB1 of hRPA70$_{1–326}$ when bound to dT$_{8}$ (red circles), the 9mer (blue squares) and dT$_{12}$ (green crosses) on the vertical axis versus residue number on the horizontal axis. (**C**) Plot showing the amide ^{15}N chemical shift changes in p.p.m. for the assigned resonances from the NTD of hRPA70$_{1–326}$ when bound to dT$_{8}$ (red circles), the 9mer (blue squares) and dT$_{12}$ (green crosses) on the vertical axis versus residue number on the horizontal axis. (**D**) Plot showing the amide ^{15}N chemical shift changes in p.p.m. for the assigned resonances from SSB1 of hRPA70$_{1–326}$ when bound to dT$_{8}$ (red circles), the 9mer (blue squares) and dT$_{12}$ (green crosses) on the vertical axis versus residue number on the horizontal axis.

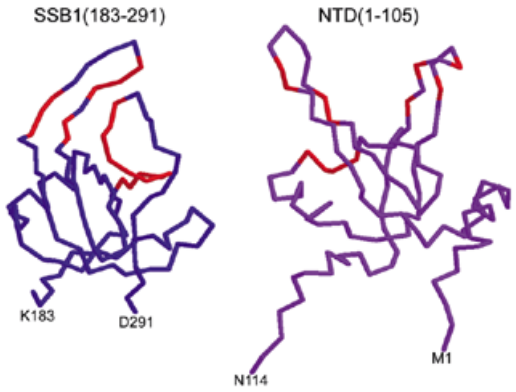

Figure 5. Ribbon diagrams showing the backbone topology for residues 183–291 of SSB1 (left) and residues 1–114 of the NTD (right). The backbone positions for residues from both domains with the largest amide ^{1}H and/or ^{15}N chemical shift changes are colored red. For SSB1 this includes residues I209–T211, R216–E218, K220, F222 and F269–T279. For the NTD this includes residues T34, T35, R41, Y42, A59–L62, T86, D89, R91, V93 and Y118. The ribbon diagram for SSB1 was adapted from the coordinates in PDB accession file 1jmc (25). The ribbon diagram for the NTD was adapted from the solution structure of hRPA70$_{1–168}$ (11).

affected by ssDNA binding. To distinguish between these two possibilities the amide ^{1}H and ^{15}N resonances of hRPA70$_{1–168}$ were monitored before and after addition dT$_{10}$ to 2 mM. The amide ^{1}H and ^{15}N chemical shift changes were similar to those observed for the NTD resonances from hRPA70$_{1–326}$ shown in Figure 4A and C. The amide ^{1}H chemical shift differences for the NTD before and after addition of dT$_{10}$ in the context of hRPA70$_{1–168}$ and before and after addition of dT$_{8}$ in the context of hRPA70$_{1–326}$ are shown in Figure 6. The amide ^{1}H chemical shift differences for the NTD in the context of hRPA70$_{1–168}$ were measured as described for Figure 4. In Figure 6 the chemical shift differences, in p.p.m., are plotted on the vertical axis and the residue numbers are plotted on the horizontal axis. In Figure 6 red circles correspond to the chemical shift changes for the NTD in the context of hRPA70$_{1–326}$ and black crosses correspond to the chemical shift changes for the NTD in the context of hRPA70$_{1–168}$. These chemical shift differences were correlated and the statistics for the correlation are listed in Table 1, correlation E. The correlation strongly suggests a similar, direct interaction between the NTD and ssDNA for both RPA fragments (31). This result is consistent with the

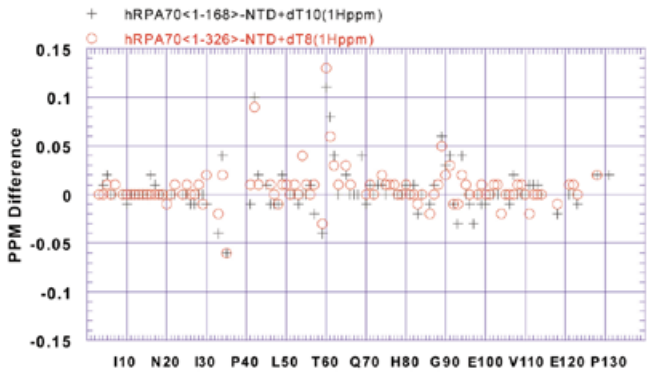

Figure 6. Plot showing the amide ^{1}H chemical shift changes in p.p.m. on the vertical axis versus residue number on the horizontal axis for the assigned resonances from the NTD of $hRPA70_{1–326}$ when bound to dT_8 (red circles) and the NTD from $hRPA70_{1–168}$ when bound to dT_{10} (black crosses).

earlier observations that showed weak coupling between the NTD and SSB1 and independent rotation of the two domains. The presence of a direct interaction between the NTD and ssDNA also suggests that the weak coupling observed between the NTD and SSB1 is not greatly affected by ssDNA binding.

The NTD and SSB1 have similar topologies

During the course of this study structural similarities between the NTD and SSB1 were observed; these similarities are in the absence of any significant sequence similarity between the two domains (32; Fig. 5). The global folds of the NTD and SSB1 are classified as 5-stranded, anti-parallel β-barrels (11,12). The distance alignment algorithm DALI was used to measure the topological similarities between the NTD and SSB1 (33). A comparison of the NTD with itself gave a DALI score of 24, while a comparison of the NTD with an SSB1 structure bound to ssDNA gave a DALI score of 4.1, with a root mean square difference (r.m.s.d.) in the average α carbon positions of 3.9 Å. According to Holm and Sander a DALI score >4 indicates significant structural similarity (33).

As expected, analysis of the amide ^{1}H and ^{15}N chemical shift changes for $hRPA70_{1–326}$ indicated a change in the structure of SSB1 when it is bound to ssDNA. It is likely that the DALI score would increase and the r.m.s.d. would decrease if the NTD structure was compared with an SSB1 structure that was not bound to ssDNA. This idea is supported by the DALI alignment between the NTD and the human mitochondrial ssDNA-binding protein, whose structure is also classified as a 5-stranded, anti-parallel β-barrel and was solved in the absence of ssDNA (34). This alignment gave a DALI score of 4.3, with a r.m.s.d. of 2.9 Å.

CONCLUSIONS

In this report NMR was used to examine the domain interactions of $hRPA70_{1–326.}$ The correlation analysis of the NTD and SSB1 demonstrated that the two domains interact weakly. Furthermore, a transverse relaxation study of $hRPA70_{1–168}$ and $hRPA70_{1–326}$ indicated that molecular tumbling of the two domains was uncorrelated. NMR was also used to examine the structural basis for ssDNA binding by $hRPA70_{1–326}$. This examination revealed that ssDNA binding altered the structures of both the NTD and SSB1. The specific chemical shift changes observed for the NTD suggested either the presence of a ssDNA-binding site or a direct interaction with SSB1. Unexpectedly, correlation analysis of NTD binding to dT_{10} verified a direct interaction between the NTD and ssDNA. Due to the structural similarity between the NTD and SSB1 we imagine that the NTD will interact with ssDNA in a comparable manner to SSB1. However, this conclusion is complicated by the lack of sequence similarity between the NTD and SSB1 and the fact that structurally dissimilar regions of the NTD and SSB1 had the largest chemical shift changes upon binding to ssDNA.

According to band shift assays, the affinity of the interaction between the NTD and ssDNA is weak and significantly less than the affinity between hRPA70 and p53, a protein known to interact primarily with the NTD (30,35,36). However, a recent analysis of the chemical shift changes that occurred when p53 was bound to the NTD suggested that p53 and ssDNA occupy overlapping sites on the NTD (Yi and Arrowsmith, unpublished results). Furthermore, it is known that ssDNA disrupts the hRPA70–p53 interaction (13). One interpretation of these results is that p53 and ssDNA are in direct competition for a binding site on the NTD. Furthermore, the flexible linker would enhance this competition by positioning the NTD in close proximity to ssDNA when SSB1 and SSB2 are tightly bound.

SUPPLEMENTARY MATERIAL

Supplementary Material is available at NAR Online.

ACKNOWLEDGEMENTS

This work was performed in the Environmental Molecular Sciences Laboratory (a national scientific user facility sponsored by the DOE Office of Biological and Environmental Research) located at Pacific Northwest National Laboratory and operated for DOE by the Battelle Corporation. The authors are grateful to G. Buchko, J. Cort and P. Vise for critically reading this manuscript. The authors also wish to thank A. Edwards for pointing out the topological similarities between the NTD and SSB1. G.W.D. and D.F.L. were supported by US Department of Energy project 24931, Budget and Reporting no. KP11-01-01-0, Structural and Functional Aspects of Nucleotide Excision Repair.

REFERENCES

1. Wold,M.S. (1997) Replication protein A: a heterotrimeric, single-stranded DNA-binding protein required for eukaryotic DNA metabolism. *Annu. Rev. Biochem.*, **66**, 61–91.
2. Ishiai,M., Sanchez,J.P., Amin,A.A., Murakami,Y. and Hurwitz,J. (1996) Purification, gene cloning and reconstitution of the heterotrimeric single-stranded DNA-binding protein from Schizosaccharomyces pombe. *J. Biol. Chem.*, **271**, 20868–20878.
3. Philipova,D., Mullen. J.R., Maniar,H.S., Gu,C. and Brill,S.J. (1996) A hierarchy of SSB protomers in replication protein. *Genes Dev.*, **10**, 2222–2233.

4. van der Knaap,E., Jagoueix,S. and Kende,H. (1997) Expression of an ortholog of replication protein A1 (RPA1) is induced by gibberellin in deepwater rice. *Proc. Natl Acad. Sci. USA*, **94**, 9979–9983.
5. Gomes,X.V., Henricksen,L.A. and Wold,M.S. (1996) Proteolytic mapping of human replication protein A: evidence for multiple structural domains and a conformational change upon interaction with single-stranded DNA. *Biochemistry*, **35**, 5586–5595.
6. Lao,Y., Gomes,X.V., Ren,Y., Taylor,J.-S. and Wold,M.S. (2000) Replication protein A interactions with DNA. III. Molecular basis of recognition of damaged DNA. *Biochemistry*, **39**, 850–859.
7. Seo,Y.-S. and Hurwitz,J. (1993) Isolation of helicase alpha, a DNA helicase from HeLa cells stimulated by a fork structure and single-stranded DNA-binding proteins. *J. Biol. Chem.*, **268**, 10282–10295.
8. He,Z., Brinton,B.T., Greenblatt,J., Hassell,J.A. and Ingles,C.J. (1993) The transactivator proteins VP16 and GAL4 bind replication factor A. *Cell*, **73**, 1223–1232.
9. Li,R. and Botchan,M.R. (1993) The acidic transcriptional activation domains of VP16 and p53 bind the cellular replication protein A and stimulate *in vitro* BPV-1 DNA replication. *Cell*, **73**, 1207–1221.
10. Dutta,A., Ruppert,J.M., Aster,J.C. and Winchester,E. (1993) Inhibition of DNA replication factor RPA by p53. Inhibition of DNA replication factor RPA by p53. *Nature*, **365**, 79–82.
11. Jacobs,D.M., Lipton,A.S., Isern,N.G., Daughdrill,G.W., Gomes,X.V., Wold,M.S. and Lowry,D.F. (1999) Human replication protein A: global fold of the N-terminal RPA-70 domain reveals a basic cleft and flexible C-terminal linker. *J. Biomol. NMR*, **14**, 321–331.
12. Bocharev,A., Pfuetzner,R.A., Edwards,A.M. and Frappier,L. (1997) Structure of the single-stranded-DNA-binding domain of replication protein A bound to DNA. *Nature*, **385**, 176–181.
13. Miller,S.D., Moses,K., Jayaraman,L. and Prives,C. (1997) Complex formation between p53 and replication protein A inhibits the sequence-specific DNA binding of p53 and is regulated by single-stranded DNA. *Mol. Cell. Biol.*, **17**, 2194–2201.
14. Henrickson,L.A., Umbricht,C.B. and Wold,M.S. (1994) Recombinant replication protein A: expression, complex formation and functional characterization. *J. Biol. Chem.*, **269**, 11121–11132.
15. Kay,L.E., Keifer,P. and Saarinen,T. (1992) Pure absorption gradient enhanced heteronuclear single quantum correlation spectroscopy with improved sensitivity. *J. Am. Chem. Soc.*, **114**, 10663–10665.
16. Zhang,O., Kay,L.E., Olivier,P. and Forman-Kay,J.D. (1994) Backbone ^{1}H and ^{15}N resonance assignments of the N-terminal SH3 domain of drk in folded and unfolded states using enhanced-sensitivity pulsed field gradient NMR techniques. *J. Biomol. NMR*, **4**, 845–858.
17. Muhandiram,D.R. and Kay,L.E. (1994) Gradient-enhanced triple-resonance three-dimensional NMR experiments with improved sensitivity. *J. Magn. Reson.*, **103B**, 203–216.
18. Wittekind,M. and Mueller,L. (1993) HNCACB, a high-sensitivity 3D NMR experiment to correlate amide-proton and nitrogen resonances with the alpha- and beta-carbon resonances in proteins. *J. Magn. Reson.*, **101B**, 201–205.
19. Grzesiek,S. and Bax,A. (1992) Correlating backbone amide and side-chain resonances in larger proteins by multiple relayed triple resonance NMR. *J. Am. Chem. Soc.*, **114**, 6291–6293.
20. Grzesiek,S. and Bax,A. (1992) Improved 3D triple-resonance NMR techniques applied to a 31kDa protein. *J. Magn. Reson.*, **96**, 432–440.
21. Miller,A.F., Papastavros,M.Z. and Redfield,A.G. (1992) NMR studies of the conformational change in human N-p21ras produced by replacement of bound GDP with the GTP analog GTP gamma S. *Biochemistry*, **31**, 10208–10216.
22. Miller,A.F., Halkides,C.J. and Redfield,A.G. (1993) An NMR comparison of the changes produced by different guanosine 5′-triphosphate analogs in wild-type and oncogenic mutant p21ras. *Biochemistry*, **32**, 7367–7376.
23. Limmer,S., Reiser,C.O., Schirmer,N.K., Grillenbeck,N.W. and Sprinzl,M. (1992) Nucleotide binding and GTP hydrolysis by elongation factor Tu from Thermus thermophilus as monitored by proton NMR. *Biochemistry*, **31**, 2970–2977.
24. Lowry,D.F., Roth,A.F., Rupert,P.B., Dahlquist,F.W., Moy,F.J., Domaille,P.J. and Matsumura,P. (1994) Signal transduction in chemotaxis. A propagating conformation change upon phosphorylation of CheY. *J. Biol. Chem.*, **269**, 26358–26362.
25. Swanson,R.V., Lowry,D.F., Matsumura,P., McEvoy,M.M., Simon,M.I. and Dahlquist,F.W. (1995) Localized perturbations in CheY structure monitored by NMR identify a CheA binding interface. *Nature Struct. Biol.*, **2**, 906–910.
26. Kay,L.E., Torchia,D.A. and Bax,A. (1989) Backbone dynamics of proteins as studied by ^{15}N inverse detected heteronuclear NMR spectroscopy: application to staphylococcal nuclease. *Biochemistry*, **28**, 8972–8979.
27. Zhou,H., McEvoy,M.M., Lowry,D.F., Swanson,R.V., Simon,M.I. and Dahlquist,F.W. (1996) Phosphotransfer and CheY-binding domains of the histidine autokinase CheA are joined by a flexible linker. *Biochemistry*, **35**, 433–443.
28. Davis,D.G., Perlman,M.E. and London,R.E. (1994) Direct measurement of the dissociation-rate constant for inhibitor-enzyme complexes via the $T_1\rho$ and T_2 (CPMG) methods. *J. Magn. Reson.*, **104B**, 266–275.
29. Peng,J.W. and Wagner,G. (1992) Mapping of spectral density functions using heteronuclear NMR relaxation measurements. *J. Magn. Reson.*, **98**, 308–322.
30. Walther,A.P., Gomes,X.V., Lao,Y., Lee,C.G. and Wold,M.S. (1999) Replication protein A interactions with DNA. 1. Functions of the DNA-binding and zinc finger domains of the 70-kDa subunit. *Biochemistry*, **38**, 3963–3973.
31. Taylor,J.R. (1982) *An Introduction to Error Analysis: The Study of Uncertainties in Physical Measurements*. University Science Books.
32. Tatusova,T.A. and Madden,T.L. (1999) BLAST 2 sequences, a new tool for comparing protein and nucleotide sequences. *FEMS Microbiol. Lett.*, **174**, 247–250.
33. Holm,L. and Sander,C. (1993) Protein structure comparison by alignment of distance matrices. *J. Mol. Biol.*, **233**, 123–138.
34. Yang,C., Curth,U., Urbanke,C. and Kang,C. (1997) Crystal structure of the human mitochondrial single-stranded DNA binding protein at 2.4 Å resolution. *Nature Struct. Biol.*, **4**, 153–157.
35. Kuhn,C., Muller,F., Melle,C., Nasheuer,H.P., Janus,F., Deppert,W. and Grosse,F. (1999) Surface plasmon resonance measurements reveal stable complex formation between p53 and DNA polymerase alpha. *Oncogene*, **18**, 769–774.
36. Lin,Y.-L., Chen,C., Keshav,K.F., Winchester,E. and Dutta,A. (1996) Dissection of functional domains of the human DNA replication protein complex replication protein A. *J. Biol. Chem.*, **271**, 17190–17198.